Sign-Singularity of the Reduced Magnetic Helicity in the Solar Wind Plasma

V. Carbone,[1,2] S. Perri,[3] E. Yordanova,[4] P. Veltri,[1] R. Bruno,[5] Y. Khotyaintsev,[4] and M. André[4]

[1]Dipartimento di Fisica, Universitá della Calabria, 87036 Rende (CS), Italy
[2]Liquid Crystal Laboratory (INFM), Ponte P. Bucci Cubo 33B, I-87036 Rende (CS), Italy
[3]International Space Science Institute, Hallerstrasse 6, CH-3012 Bern, Switzerland
[4]Swedish Institute of Space Physics, Uppsala, Sweden
[5]Istituto di Fisica dello Spazio Interplanetario/INAF, via Fosso del Cavaliere Roma, Italy

(Received 27 October 2009; published 7 May 2010)

We investigate the scaling laws of a signed measure derived from the reduced magnetic helicity which has been determined from Cluster data in the solar wind. This quantifies the handedness of the magnetic field; namely, it can be related to the polarization of the magnetic field fluctuations (right or left hand). The measure results to be sign-singular; that is, we do not observe any scale-dependent effect at the ion- and at electron-cyclotron frequencies. Cancellations between right- and left-hand polarizations go on in the dispersive or dissipative range, beyond the electron-cyclotron frequency. This means that the mechanism responsible for the generation of the dispersive or dissipative range is rather insensitive to the polarization of the magnetic field fluctuations.

DOI: 10.1103/PhysRevLett.104.181101 PACS numbers: 96.50.Ci, 52.35.Ra, 89.75.Da, 94.05.Lk

Interplanetary space is permeated by solar wind, a continuous flow of plasma flowing away from the Sun [1]. The solar wind is in a high turbulent state, and spacecraft data represent a unique opportunity to investigate plasma turbulence in a natural environment [2,3]. Spacecraft observations of plasma turbulence show that in the low-frequency range, $f < f_{\rm ci}$ ($f_{\rm ci}$ is a characteristic frequency associated with the ion-cyclotron scale $\lambda_{\rm ci} = v_{\rm th}/\omega_{\rm pi}$, being $\omega_{\rm pi}$ the ion gyro-frequency and $v_{\rm th}$ the ion thermal speed), the magnetic spectrum follows a power law $f^{-5/3}$, which represents a Kolmogorov-like turbulent energy cascade [3,4]. For high-frequency fluctuations, $f > f_{\rm ci}$, the spectrum steepens significantly to $f^{-\alpha}$ [5–7] with a slope in the range $\alpha \in [2, 4]$. The high-frequency part of the spectrum is either associated to a dissipative range, as in nonmagnetized fluids [5,6,8,9], or to a different turbulent energy cascade [7,10–12] caused by dispersive effects [13–16]. Recently, using both the search-coil (STAFF) [17] and the flux-gate magnetometer (FGM) [18] instruments onboard Cluster, it has been shown that the magnetic energy spectrum falls off exponentially beyond the electron-cyclotron frequency $f_{\rm ce}$ [19], which is probably the starting point of a dissipative range. Therefore, understanding the formation of the high-frequency part of the spectrum is a compelling topic for plasma physics. In fact, in the solar wind, the mean free path is roughly equal to the Sun–Earth distance so that the dissipation via collisions is negligible. Damping mechanisms, such as wave-particle interactions, are then required.

In order to understand the nature of small-scale turbulence, we investigate the behavior of the normalized magnetic helicity [20]. This quantity is related to the polarizations of the magnetic field fluctuations. At low frequencies, it oscillates around zero, while at high frequencies, it assumes a defined sign [5,21]. This evidence would mean that one of the polarizations is canceled out by dispersive or dissipative effects, like cyclotron or nonresonant damping. Although numerical simulations show that the Landau damping saturates nonlinearly for finite amplitude fluctuations [22], the presence of a negative value of the normalized magnetic helicity has been considered consistent with the cyclotron damping of the Alfvén waves [5].

The helicity of the magnetic field fluctuations, $H = \mathbf{A}\cdot\mathbf{B}$ (where $\mathbf{A}$ is the vector potential and $\mathbf{B} = \nabla\times\mathbf{A}$) is a measure of the linkage of flux tubes or of the lack of mirror symmetry [23]. The total magnetic helicity on a given volume V can be calculated as the Fourier transform of the symmetric part of the correlation tensor between $\mathbf{A}$ and $\mathbf{B}$ [20], that is

$$H_m = \int \mathbf{A}\cdot\mathbf{B}d^3\mathbf{x} \equiv \int d^3\mathbf{k}H_{jj}(\mathbf{k}) \tag{1}$$

where $H_{jj}(\mathbf{k})$ is the spectrum of the magnetic helicity. However, from the observations, we can calculate only the reduced magnetic helicity, that is, the integration in Eq. (1) is only along the direction of the flow. In addition, because the solar wind flow is superAlfvénic, the magnetic field fluctuations, travelling typically at the Alfvén speed, can be considered "frozen-into" the bulk flow and the so-called *Taylor's hypothesis* [24] is applicable. The time variations in the field detected by spacecraft are simply related to variations in space, i.e., $\delta r = V_{\rm SW}\delta t$, and thus, $k = \omega/V_{\rm SW}$. If x is the direction of the flow motion, we can define the normalized reduced helicity at frequency ω as

$$H_m^{(r)}(\omega) = \frac{2\,\mathrm{Im}\{B_y^\star(\omega)B_z(\omega)\}}{|B_y(\omega)|^2 + |B_z(\omega)|^2}, \tag{2}$$

which is bounded in the range $-1 \le H_m^{(r)} \le 1$. Defining a

TABLE I. Plasma parameters for both Cluster and Helios 2 data sets: the magnetic field intensity, the bulk speed, the proton number density n_p, the proton temperature T_p, and the ions and electron Doppler-shifted frequencies f_{ci} and f_{ce}.

	Set A	Set B	0.3 AU	0.7 AU	0.9 AU
$\langle \mathbf{B} \rangle$ (nT)	8	4	42	11	7
$\mathbf{v}$ (km/s)	350	670	700	630	650
n_p (cm^{-3})	29	3	62.2	13.5	8
T_p (eV)	7	25	48	23	18
β	1.3	1.6	0.7	1.1	1.3
f_{ci} (Hz)	0.71	0.38	0.1	0.1	0.1
f_{ce} (Hz)	31.0	16.4			

signed measure for the reduced magnetic helicity, we can quantify the scaling properties of the polarizations of the magnetic field fluctuations. A signed measure is defined considering a sequence $H_m^{(r)}(\omega)$ over a length Ω and a hierarchy $\Omega_i(f)$ of disjoint subintervals of increasing size f spanning over the all set Ω. At the ith interval, at the scale f, the signed measure is defined as

$$\mu_i(f) = \frac{\int_{\Omega_i} H_m^{(r)}(\omega) d\omega}{\int_{\Omega} |H_m^{(r)}(\omega)| d\omega}. \tag{3}$$

At variance to the probability measure, the signed measure over a finite interval can assume both positive and negative values [25]. The presence of cancellations of both polarizations at small scales can be characterized by a single scaling exponent κ, named cancellation exponent [26], which is related to the geometry of small-scale structures [27]. This quantity can be defined through the scaling behavior of the partition function $\chi(f) \equiv \sum_i |\mu_i(f)| \sim f^{\kappa}$ (the sum is extended to all the subintervals at a given scale $\tau \sim 1/f$). The scaling exponent κ is a measure of how fast positive and negative contributions cancel down at different scales. Sign-singularity, $\kappa > 0$, is then realized when cancellations between positive and negative $H_m^{(r)}(f)$ values are reduced for small scales. For a Brownian process with uncorrelated steps $\kappa = 1/2$, while trivially $\kappa = 0$ for a positive measure. Once structures with a single sign of reduced magnetic helicity are dominant in the integral in (3), the partition function $\chi(f)$ tends to saturate, meaning that a plateau appears in the shape of $\chi(f)$ for scales smaller than a typical saturation scale, $1/f_{\mathrm{sat}}$. Sign-singularity has been observed in turbulent fields and in other random phenomena [26,28,29], in the current helicity in the solar photosphere [30], and in the helicity of large scale turbulence in space [31].

Two data sets from both the FGM and the STAFF instruments on board Cluster have been analyzed. The first data set refers to the period 00:07-02:40 UT on 2002 February 19 (hereafter, data set A) during the solar maximum; the second data set is relevant to 00:00-00:40 UT on 2007 January 30 (hereafter, data set B) during the declining phase of solar cycle 23. The data in set A are sampled at frequency $\Delta\omega = 22$ Hz (i.e., a sampling time of $\Delta t = 0.045$ sec) for FGM, and at frequency $\Delta\omega = 25$ Hz (i.e., $\Delta t = 0.040$ sec) for STAFF. For the data set B, we analyze magnetic field data measured at a sampling frequency $\Delta\omega = 67$ Hz (i.e., $\Delta t = 0.015$ sec) for FGM, and at $\Delta\omega = 450$ Hz (i.e., $\Delta t \simeq 0.0022$ sec) for STAFF. The higher sampling rate allows us to perform analysis in the high-frequency part of the power spectrum, i.e., in the dispersive or dissipative range. For comparison, we analyze the 6 sec resolution Helios 2 data; that is, we investigate cancellations at large scales, in the inertial range. Three periods at three different heliocentric distances, i.e., $R = 0.3, 0.7, 0.9$ AU, have been selected, corresponding to fast streams. All the data sets shown are in the local s/c right–handed reference frame (RTN), where R indicates the radial Sun-spacecraft antisunward direction, T represents the tangential direction, which is calculated as the cross product between the solar rotation axis and the R direction, and N completes the frame. In Table I, the mean plasma parameters are reported for the data set A and B and for the Helios 2 data sets. Notice that the data set A is a low speed stream with a slightly lower plasma β and a lower proton temperature T_p, while the data set B refers to a fast stream with a higher proton temperature and a slightly higher β.

We computed power spectra for the magnetic field components and for the magnetic field magnitude for the data sets A and B. The slopes α of the power spectra of the magnetic field magnitude are displayed in Table II along with the ranges of frequencies in which fits have been performed.

TABLE II. Spectral slopes α of the power spectra of the magnetic field magnitude and cancellation exponents κ for the data sets A and B. Errors are of the order of 10^{-3}.

	Data set A				Data set B			
	FGM		STAFF		FGM		STAFF	
	α	κ	α	κ	α	κ	α	κ
$[f_1 - f_2]$ Hz	[0.01–0.2]	[0.01–1.0]	[1–10]	[0.8–10]	[0.01–0.2]	[0.01–1]	[1–17]	[1–50]
$s/c1$	1.58	0.351	2.54	0.369	1.46	0.362	2.71	0.406
$s/c2$	1.58	0.392	2.65	0.364	1.44	0.356	2.78	0.414
$s/c3$	1.56	0.407	2.62	0.377	1.39	0.366	2.84	0.408
$s/c4$	1.59	0.427	2.61	0.363	1.38	0.338	2.80	0.400

In data set A, FGM data are suitable for analysis up to 1 Hz, while STAFF data allow us to go down towards 10 Hz. We have not considered the largest scales, typically below 0.01 Hz for FGM and below 0.5 Hz for STAFF, to avoid border effects. In data set B, FGM data are used up to 1 Hz (at higher frequencies a flattening in the spectra is observed), while the STAFF instrument provides data up to 180 Hz (at this frequency, a low-pass filter has been applied). However, we consider a high-frequency range for our data analysis ranging from 1 to 50 Hz.

In Fig. 1, the values of the partition function $\chi(f)$, calculated from the FGM Cluster 2 (C2) data (stars) and from the STAFF C1 data (circles), as a function of the frequency f, for the data set A are displayed in the top panel. $\chi(f)$ values computed from the C3 data for the data set B are shown in the bottom panel. The displayed error bars have been estimated as the standard deviation of the partition function $\chi(f)$. The vertical dashed lines indicate both the Doppler-shifted ion-cyclotron $f_{\rm ci}$ and electron-cyclotron $f_{\rm ce}$ frequencies, calculated under the assumption of the Taylor's hypothesis [19]. All the trends are well fitted by power laws (solid lines in Fig. 1) with a characteristic index $\kappa > 0$, indicating that the measure is sign-singular. A similar power law behavior has been found for the other s/c, and the relevant slopes are reported in Tables II (the frequency ranges in which cancellations have been calculated are also indicated). The typical slopes found are significantly smaller than $\kappa = 1/2$, thus indicating the presence of smooth structures. The cancellation exponents for the data set A are slightly different from those computed from the data set B, probably due to the differences in the plasma parameters. To improve the statistics of our results, we have analyzed two additional periods of Cluster measurements (22:00-22:30 UT on 2005 April 28, and 13:20-14:00 UT on 2007 January 20). We have obtained the same behavior of the partition function and similar values of the scaling exponents to the reported ones above. It is worth noticing that the partition function does not saturate, meaning that the measure is sign-singular, independent of the presence of both the ion-cyclotron and the electron-cyclotron frequencies. Cancellations between both polarizations occur at frequencies higher than both ion-cyclotron and electron-cyclotron frequencies without a net predominance of a given polarization.

The computation of the partition function $\chi(f)$ has also been performed for the Helios 2 data sets in the fast wind. Figure 2 displays cancellations as a function of the frequency for the three data sets. The curves shown have been separated for readability. The κ values are shown in the figure legend. There are no significant differences among them; therefore, the process of cancellations of polarizations seems to be independent of the radial distance [21]. It is worth noticing that all the three Helios data sets refer to fast streams having values of the plasma beta roughly similar; therefore, the slopes of the partition function are very close to each other, i.e., $\kappa \simeq 0.44$. Further, the values of κ found for the fast streams detected by Helios 2 are

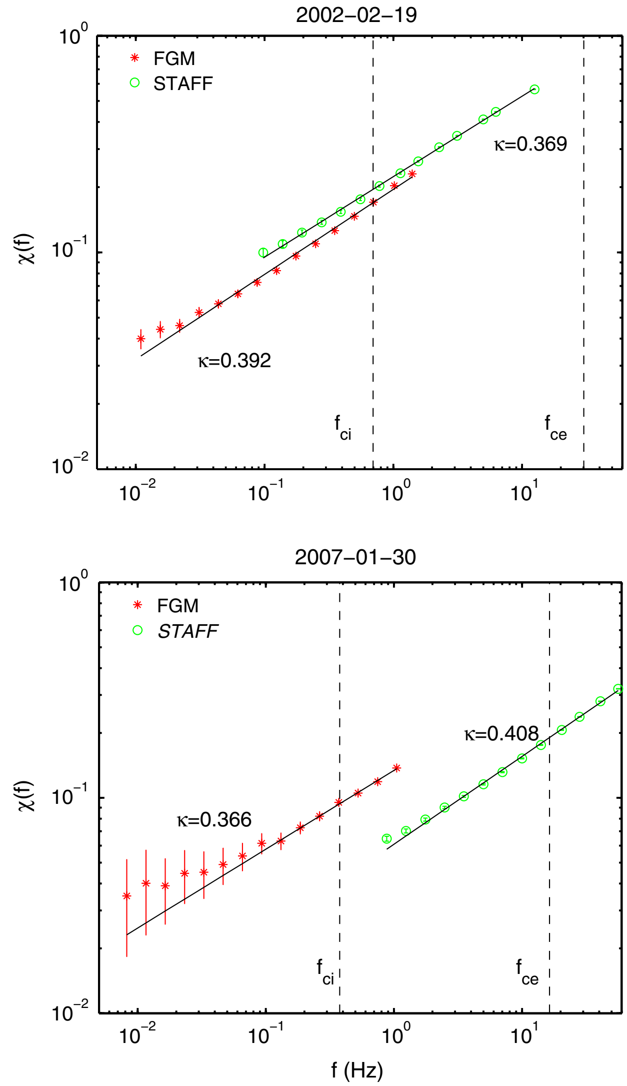

FIG. 1 (color online). Partition functions vs frequency in log-log axis for the data set A and for the data set B. Cancellations are calculated from FGM Cluster2 data (stars) and from STAFF C1 data (circles) for the data set A, while from the C3 s/c for the data set B (symbols as indicated). The Doppler-shifted ion-cyclotron $f_{\rm ci}$ and the electron-cyclotron $f_{\rm ce}$ frequencies are plotted (vertical dashed lines). Linear fits are also shown (solid black lines).

quite close to 0.5 that is, to the value expected for a random process. This confirms the quasistochastic nature of the magnetic field fluctuations in the fast wind at large scales [32].

To summarize, in this Letter, we investigated the scaling behavior of the reduced magnetic helicity, which is related to the sign of polarization of the magnetic field fluctuations. The results shown here are in agreement with the behavior of the reduced magnetic helicity found by Refs. [5,21] in the inertial range of the magnetic turbulence in the solar wind: $H_m^{(r)}(f)$ is quasirandomly oscillating between ± 1. Indeed, the reduced magnetic helicity is found to be sign-singular; that is, a power law growth has

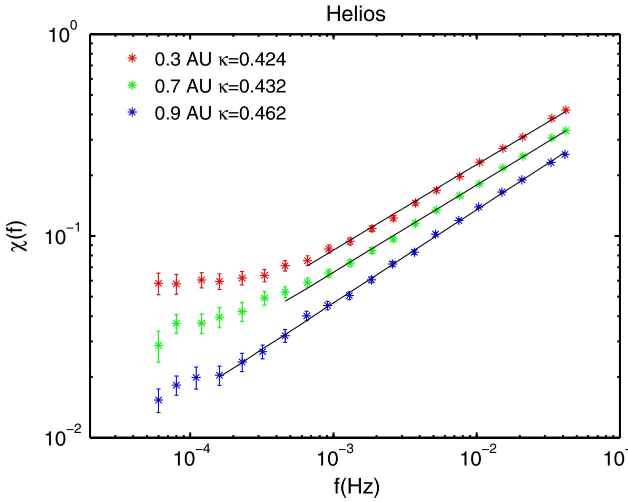

FIG. 2 (color online). Same as Fig. 1 but for the Helios 2 data sets at 0.3 AU, 0.7 AU, and 0.9 AU. The three curves have been displaced from each other for readability. Solid black lines indicate the best linear fits.

been observed for the partition function $\chi(f)$ with a scaling exponent $\kappa \leq 1/2$. However, the high resolution data analyzed here show that this quasirandom oscillation of the reduced magnetic helicity continues even in the high-frequency part of magnetic turbulence, indicating that both the left- and the right-hand polarized waves survive. Therefore, the cyclotron damping interpretation of dispersive range [5,11,12,21], which assumes that the high-frequency fluctuations are dominated by right-handed polarized whistler or fast fluctuations due to dissipation of left-handed polarized fluctuations by cyclotron resonance, clearly cannot be in agreement with our analysis. A competing mechanism for the generation of the dispersive region [33], involving the presence of a net flux of right-handed kinetic Alfvén waves (KAW) [34], is also inconsistent with observations. However, in the case of close to zero cross helicity, a flux of oppositely directed Alfvén waves should be present at small scales [35]; in this case, the presence of KAW should give rise to the observed behavior of cancellations. Finally, it is worth noticing that the results shown here can also be in agreement with the presence of a dispersive region of strong magnetic field fluctuations anticorrelated with density fluctuations and decoupled from velocity fluctuations generated by the Hall effect, observed both in numerical simulations and in the magnetopause region [15,36].

This work is partially financed by Italian Space Agency, Contract ASI No. I/015/07/0 "Esplorazione del Sistema Solare." E. Y. thanks ISSI for the support of her visit while preparing this manuscript.

[1] A. J. Hundhausen, *Coronal Expansion and Solar Wind* (Springer, New York, 1972).
[2] C.-Y. Tu and E. Marsch, Space Sci. Rev. **73**, 1 (1995).
[3] R. Bruno and V. Carbone, Living Rev. Solar Phys. **2**, 4 (2005).
[4] L. Sorriso-Valvo *et al.*, Phys. Rev. Lett. **99**, 115001 (2007).
[5] R. J. Leamon *et al.*, J. Geophys. Res. **103**, 4775 (1998).
[6] C. W. Smith *et al.*, Astrophys. J. **645**, L85 (2006).
[7] O. Alexandrova *et al.*, Astrophys. J. **674**, 1153 (2008).
[8] R. J. Leamon *et al.*, J. Geophys. Res. **104**, 22331 (1999); R. J. Leamon *et al.*, Astrophys. J. **537**, 1054 (2000).
[9] S. D. Bale *et al.*, Phys. Rev. Lett. **94**, 215002 (2005).
[10] S. Ghosh *et al.*, J. Geophys. Res. **101**, 2493 (1996).
[11] O. Stawicki, S. P. Gary, and H. Li, J. Geophys. Res. **106**, 8273 (2001).
[12] H. Li, S. P. Gary, and O. Stawicki, Geophys. Res. Lett. **28**, 1347 (2001).
[13] D. Biskamp, E. Schwarz, and J. F. Drake, Phys. Rev. Lett. **76**, 1264 (1996).
[14] F. Sahraoui *et al.*, Phys. Rev. Lett. **96**, 075002 (2006).
[15] S. Servidio *et al.*, Planet. Space Sci. **55**, 2239 (2007).
[16] S. Galtier and E. Buchlin, Astrophys. J. **656**, 560 (2007).
[17] N. Cornilleau-Wehrlin *et al.*, Space Sci. Rev. **79**, 107 (1997).
[18] A. Balogh *et al.*, Space Sci. Rev. **79**, 65 (1997).
[19] F. Sahraoui *et al.*, Phys. Rev. Lett. **102**, 231102 (2009).
[20] W. H. Matthaeus *et al.*, Phys. Rev. Lett. **48**, 1256 (1982).
[21] M. L. Goldstein, D. A. Roberts, and C. A. Fitch, J. Geophys. Res. **99**, 11519 (1994).
[22] R. De Marco, V. Carbone, and P. Veltri, Phys. Rev. Lett. **96**, 125003 (2006).
[23] H. K. Moffat, *Magnetic Field Generation in Electrically Conducting Fluids* (Cambridge Univ. Press, Cambridge, 1978).
[24] G. I. Taylor, Proc. R. Soc. A **164**, 476 (1938).
[25] P. R. Halmos, *Measure Theory* (Springer Verlag, New York, 1074).
[26] E. Ott *et al.*, Phys. Rev. Lett. **69**, 2654 (1992).
[27] L. Sorriso-Valvo *et al.*, Phys. Plasmas **9**, 89 (2002).
[28] S. I. Vainshtein, Y. Du, and K. R. Sreenivasan, Phys. Rev. E **49**, R2521 (1994).
[29] V. Carbone, Europhys. Lett. **29**, 377 (1995); V. Carbone *et al.*, Europhys. Lett. **32**, 31 (1995).
[30] V. I. Abramenko, V. B. Yurchishin, and V. Carbone, Astron. Astrophys. **334**, L57 (1998); V. I. Abramenko, V. B. Yurchishin, and V. Carbone, Sol. Phys. **178**, 35 (1998); V. B. Yurchishin, V. I. Abramenko, and V. Carbone, Astrophys. J. **538**, 968 (2000).
[31] V. Carbone and R. Bruno, Astrophys. J. **488**, 482 (1997).
[32] R. Bruno *et al.*, J. Geophys. Res. **108**, 1130 (2003).
[33] G. G. Howes *et al.*, Phys. Rev. Lett. **100**, 065004 (2008); A. A. Schekochihin *et al.*, Astrophys. J. Suppl. Ser. **182**, 310 (2009).
[34] G. G. Howes and E. Quataert, Astrophys. J. **709**, L52 (2010).
[35] B. D. G. Chandran, Astrophys. J. **685**, 646 (2008).
[36] K. Stasiewicz *et al.*, Phys. Rev. Lett. **90**, 085002 (2003).